Scripta Materialia 149 (2018) 58–61

Contents lists available at ScienceDirect

Scripta Materialia

journal homepage: www.elsevier.com/locate/scriptamat

Regular article

Densification effects on porous silica: A molecular dynamics study

Ye Tian [a,b], Jincheng Du [b,*], Dongxia Hu [a], Wanguo Zheng [a], Wei Han [a,c,*]

[a] Research Center of Laser Fusion, China Academy of Engineering Physics, Mianyang 621900, China
[b] Department of Material Science and Engineering, University of North Texas, Denton, TX 76203, USA
[c] Collaborative Innovation Center of IFSA, Shanghai Jiao Tong University, Shanghai 200240, China

ARTICLE INFO

Article history:
Received 14 January 2018
Received in revised form 9 February 2018
Accepted 11 February 2018
Available online xxxx

Keywords:
Molecular dynamics simulations
Porous silica
Densification

ABSTRACT

Molecular dynamics simulations are performed to investigate the effects of hydrostatic and shock densification on the structural and mechanical properties of porous silica. In the 0–35 GPa pressure range, the equation of state reveals a unique plastic-elastic transition for this material, resulting in a continuous density increase followed by saturation. Structural modifications are reflected in the medium-range order only, as evidenced by the increase of inter-tetrahedral bond angles occurring through the pressure-induced rearrangement of Si—O—Si planes and associated bonds. Discontinuous evolution of the elastic moduli for densified porous silica is observed and associated with the change of ring statistics.

Laser-induced breakdown of large, high-quality optical elements remains a major concern in the development of inertial confinement fusion (ICF) facilities [1,2]. In the ultraviolet regime (351 nm), damage craters initiated by high-fluence, nanosecond laser irradiation on sol-gel derived silica films have been extensively observed, revealing the presence of localized microexplosions triggered by shock propagation from hot dense plasmas [3–5]. Such rapid events could in turn compress the porous material and thus lead to severe deterioration that hinders safe operation of the downstream system. While the mechanism of laser damage has been studied for decades, the interrelated structural and physical modifications of porous silica in this high-pressure process are not fully understood, which necessitates an accurate determination of the equation of state (EOS).

Determining the response of porous silica to densification is challenging as some amorphous materials are known to display anomalous behavior under high pressure. In particular, permanent density increase has been identified for vitreous silica compressed beyond 10 GPa [6–9]. As for porous silica, however, the EOS is further complicated by the pores wide size distributions which make experimental characterization challenging. Due to the success in atomic-scale modeling, molecular dynamics (MD) simulations have been applied to reproduce porous silica under ambient conditions [10–15]. For example, the creative work by Kieffer et al. and Nakano et al. has established fractal silica structures with desirable porosities via successive volume expansion [11,12]. More recently, Beckers et al. have proposed an alternative approach to generate channeled pore morphology as commonly expected in sol-gel processing [13–15]. Following previous studies, this letter investigates the effects of densification on porous silica with a series of equilibrium MD simulations to gain insights into the high-pressure products with respect to damaged silica films.

Generated using the pairwise potential developed by Teter, the undensified porous silica was created by the charge-scaling method in steps of 1 fs [13–15]. To begin 500 $Si^{+0.48}$ and 1000 $O^{-0.24}$ atoms were randomly inserted in a $31.2 \times 31.2 \times 31.2$ Å^3 periodic cube to form a 1.14 g/cm^3 supercell, the density of which is close to those of the porous silica films applied to experiments. The starting configuration was then thermalized at 300 K in the NVT ensemble, with the ionic charges successively increased to 2.4e and −1.2e for the Si and O atoms, respectively. After relaxation and equilibration at 300 K and 0 GPa, the silicate system was stabilized at 1.4 g/cm^3, corresponding to 40% porosity as the predicted density of the vitreous silica backbone is 2.3 g/cm^3 [16]. This slight density overestimation for the simulated sample as compared with the experimental films is not problematic as the structural differences for porous silica of porosities 40%–60% have been shown to be small [15].

In order to produce discrete high-density phases, hydrostatic and shock loadings were individually imposed on the porous silica sample for cross-sectional comparisons. The hydrostatic loading was conducted at 300 K in the 0–35 GPa range, where the Nose-Hoover thermostat and barostat were used in the NPT ensemble for compression. For the shock simulations, equivalent pressure was achieved by temperature-rescaling in the Hugoniot ensemble, based on the algorism proposed by Ravelo et al. [17]. Compression of each sample was performed for 100 ps, corresponding to strain rates ranging from 3.2×10^{-4} to 2.6×10^{-3} ps^{-1}. Although such strain rates are typically more than twelve orders of magnitude higher than those used in conventional experiments of static densification, stabilized structures can be effectively achieved in MD simulations, with the densities equilibrated within ~30 ps. Moreover, rapid densification is necessary for shock simulations

* Corresponding authors.
E-mail addresses: jincheng.du@unt.edu (J. Du), tonyhan2000@126.com (W. Han).

https://doi.org/10.1016/j.scriptamat.2018.02.007
1359-6462/

as compression with respect to laser-induced damage is known to occur within a few nanoseconds [3–5]. Once fully densified, all the samples were depressed back to 0 GPa, followed by structural analysis in the NVE ensemble. Viewed as a zero-porosity example, a vitreous silica bulk built through the melt-quench technique was depressed from various hydrostatic pressure to highlight the role of voids acting in densification [18].

The final densities relaxed at 0 GPa are plotted as a function of the loaded pressure in Fig. 1 to reproduce the EOS for vitreous and porous silica. In the plastic region, both materials experience continuous increase in density with pressure until a stable high-pressure state is reached. For the two compression schemes, the density of porous silica evolves similarly, which differs significantly from the trend displayed by vitreous silica. In consistent with the previous studies, the irreversible densification for vitreous silica starts from 6–10 GPa, whereas porous silica exhibits no elastic-plastic transitions, as seen from the sharp density increase in the EOS profile [19,20]. In addition, the saturation pressure for porous silica, also serving as the threshold of elastic response for the pressure-derived high-density state, lies at 12 GPa, which is about 15 GPa smaller in comparison with the densified vitreous silica. Despite the lack of antecedent structural depiction, the instability of porous silica is not surprising considering the weakening effect of the channeled pores on network connectivity.

It is essential to note from Fig. 1 that the density limit at 2.72 g/cm^3 produced by maximum densification for vitreous silica, in good agreement with the experimental measurements, is approximately equal to that for porous silica [19,20]. To extract real-space structural information of these fully compressed states and their undensified precursors, the pair distribution functions (PDF) were calculated. It has been found from the peak positions of the PDFs (not shown) that the Si—O bond length, the O—O and Si—Si pair distances for each species remain constant to be 1.6 Å, 2.6 Å and 3.1 Å, respectively. Furthermore, integrations of these primary peaks all yield a coordination number of about 4.0 for Si and 2.0 for O on average. From the radial point of view, therefore, the densification procedure does not stimulate modifications on the short-range order.

Assuming a cutoff bond length of 2.2 Å, the medium-range order is expressed in terms of the average bond angles, the dependence of which on density are shown in Fig. 2(a). The average O—Si—O angle at 109.3° keeps its value for each sample, whereas the average Si—O—Si angle in porous silica, which is initially 6° smaller than that for vitreous silica due to the small rings formed in the pores, shifts linearly towards 146° and 149° for the compressed and shocked states, respectively. Interpreted by the linear fitting procedure, the distinction in Si—O—Si angles indicates that for a given compaction ratio of porous silica, shocks indeed produce different phases from those evolve under high hydrostatic pressures. By sharp contrast, the average Si—O—Si angle in densified vitreous silica continuously decreases from 151° towards 146°, resulting in an identical value to that for the hydrostatically compressed porous silica at ~2.72 g/cm^3, even though these two samples have different initial structures and paths of density evolution under high pressure. In this regard, the pores appear to have no effect on the highest-density states of silica upon hydrostatic loading.

A Si—O—Si angle is known to change via two coupled mechanisms in irreversible densification: plane reorientation and bond swapping, which can be tracked by the time correlation of Si—O—Si plane normal vectors and the proportion of recoordinated O atoms, respectively [21,22]. Taken the undensified porous silica sample for reference, the average plane normal correlation functions, as shown in Fig. 2(b), both decrease continuously from unity to zero in a roughly linear manner, indicating a rotation from 0° to 90° by average for an oxygen-related plane. Given the changed bonding sequence, such plane bridged by an O atom with its bonding neighbors may not correspond to the same Si pair after compression. Hence, the correlation indeed monitors the overall degree to which the O atoms are adjusted to enable phase transition. Despite the similar planar evolution, the proportion of O

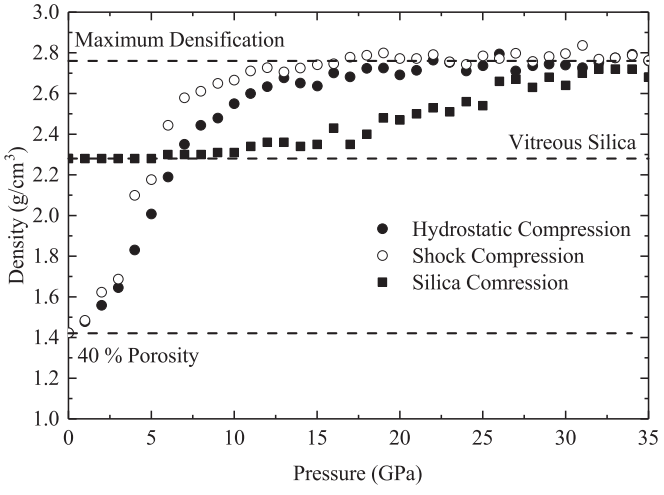

Fig. 1. Depressed density plotted versus compression pressure for porous and vitreous silica. The initial and final densities are marked with dash lines.

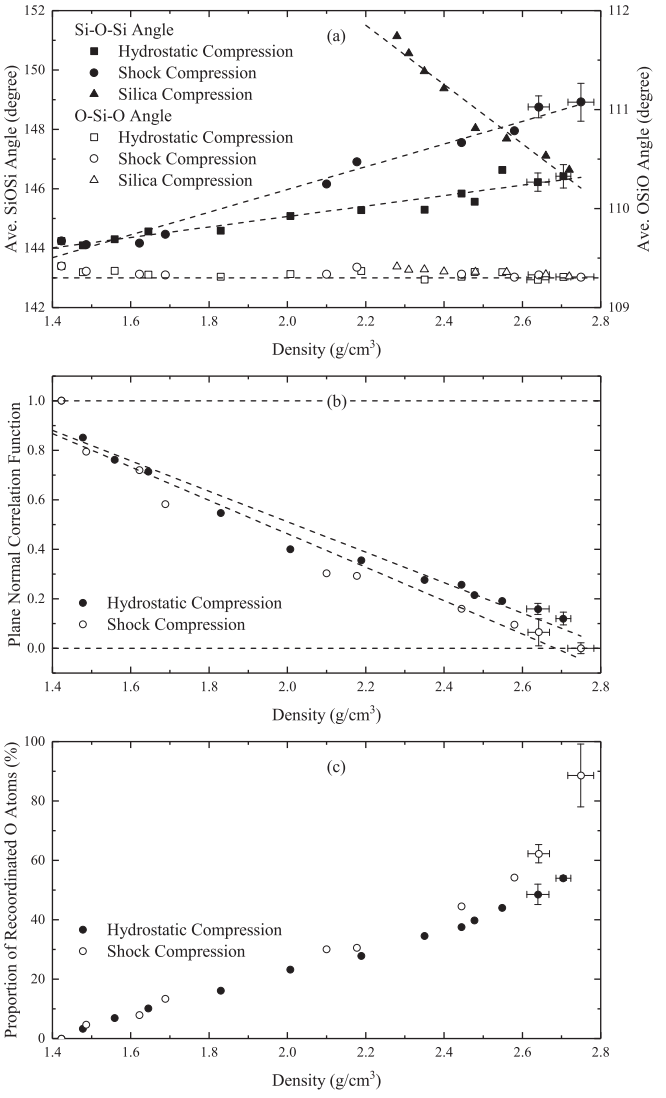

Fig. 2. (a) Average Si—O—Si and O—Si—O bond angles plotted for densified vitreous and porous silica; (b) Si—O—Si plane normal correlation function and (c) the proportion of recoordinated O atoms for densified porous silica.